Towards Understanding the Working Mechanism of Text-to-Image Diffusion Model

Mingyang Yi[1*], **Aoxue Li**[2*], **Yi Xin**[3*], **Zhenguo Li**[2]
[1] Renmin University of China
[2] Huawei Noah's Ark Lab
[3] Nanjing University
{yimingyang@ruc.edu.cn}
{liaoxue2,li.zhenguo}@huawei.com
xinyi@smail.nju.edu.cn

Abstract

Recently, the strong latent Diffusion Probabilistic Model (DPM) has been applied to high-quality Text-to-Image (T2I) generation (e.g., Stable Diffusion), by injecting the encoded target text prompt into the gradually denoised diffusion image generator. Despite the success of DPM in practice, the mechanism behind it remains to be explored. To fill this blank, we begin by examining the intermediate statuses during the gradual denoising generation process in DPM. The empirical observations indicate, the shape of image is reconstructed after the first few denoising steps, and then the image is filled with details (e.g., texture). The phenomenon is because the low-frequency signal (shape relevant) of the noisy image is not corrupted until the final stage in the forward process (initial stage of generation) of adding noise in DPM. Inspired by the observations, we proceed to explore the influence of each token in the text prompt during the two stages. After a series of experiments of T2I generations conditioned on a set of text prompts. We conclude that in the earlier generation stage, the image is mostly decided by the special token `[EOS]` in the text prompt, and the information in the text prompt is already conveyed in this stage. After that, the diffusion model completes the details of generated images by information from themselves. Finally, we propose to apply this observation to accelerate the process of T2I generation by properly removing text guidance, which finally accelerates the sampling up to 25%+.

1   Introduction

In real-world application, the Text-to-Image (T2I) generation has long been explored owing to its wide applications [47, 31, 32, 2, 15], whereas the Diffusion Probabilistic Model (DPM) [12, 37, 32] stands out as a promising approach, thanks to its impressive image synthesis capability. Technically, the DPM is a hierarchical denoising model, which gradually purifies noisy data from a standard Gaussian to generate an image. In the existing literature [31, 34, 28, 6], the framework of (latent) Stable Diffusion model [31] is a backbone technique in T2I generation via DPM. In this approach, the text prompt is encoded by a CLIP text encoder [30], and injected into the diffusion image decoder as a condition to generate a target image (latent encoded by VQ-GAN in [31]) that is consistent with the text prompt. Though this framework works well in practice, the working mechanism behind it, especially for the text prompt, remains to be explored. Therefore, in this paper, we systematically explore the working mechanism of stable diffusion.

---

[*]equal contribution
[†]corresponding to Mingyang Yi: yimingyang@ruc.edu.cn

38th Conference on Neural Information Processing Systems (NeurIPS 2024).

Our investigation starts from the intermediate status of the denoising generation process. Through an experiment (details are in Section 4), we find that in the early stage of the denoising process, the overall shapes of generated images (latent) are already reconstructed. In contrast, the details (e.g., textures) are then filled at the end of the denoising process. To explain this, we notice that the overall shape (resp. semantic details) is decided by low-frequency (resp. high-frequency) signals [9]. We both empirically show and theoretically explain that in contrast to the high-frequency signals, the low-frequency signals of noisy data are not corrupted until the end stage of the forward noise-adding process. Therefore, its reverse denoising process firstly recovers the low-frequency signal (so that overall shape) in the initial stage, and then recovers the high-frequency part in the latter stage.

Following the phenomenons, we investigate the effect of encoded tokens in the text prompt of T2I generation during the two stages, where each token is encoded by an auto-regressive CLIP text encoder. The text prompt has a length of 76, and is enclosed by special tokens [SOS] and [EOS], [†] at the beginning and end of the text prompt, respectively. Therefore, we categorize the tokens into three classes, i.e., [SOS], semantic tokens, and [EOS]. Notably, the special token [SOS] does not contain information, due to the auto-regressive encoding of the text prompt. Thus, our investigations into the influence of tokens will primarily focus on the semantic tokens and [EOS]. Surprisingly, we find that compared with semantic tokens, the special token [EOS] has a larger impact during generation.

Concretely, under a set of collected text prompts, we select 1000 pairs "[SOS] + Prompt A (B) + [EOS]$_{A(B)}$" from it. Then, replace the special token [EOS]$_A$ in the text prompt A with [EOS]$_B$ from prompt B to observe the generated data under this condition. Interestingly, we find that the generated images are more likely to be aligned with text prompt B (especially for the shape features) instead of A, so that [EOS] has a larger impact compared with semantic tokens. Besides that, we further find that the information in [EOS] is already conveyed during the early shape reconstruction stage of the denoising process. Exploring along the working stage of [EOS], we further verify and explain that the whole text prompts (including semantic ones) primarily work on the early denoising process, when the overall shapes of generated images are constructed. After that, the image details are mainly reconstructed by the images themselves. This phenomenon is explained by "first shape then details", as the injected text prompt implicitly penalizes the generated images to be consistent with it. Therefore, the penalization quickly becomes weak, when the overall shape of image is reconstructed.

Finally, we apply our observations in one practical cases: Training-free sampling acceleration, as the text prompt works in the first stage of denoising process, we remove the textual prompt-related model propagation ($\epsilon_{\theta}(t, \boldsymbol{x}_t, \mathcal{C})$ in (3)) during the details reconstruction stage, which merely change the generated images but save about 25%+ inference cost.

We summarize our contributions as follows.

1. We show, during the denoising process of the stable diffusion model, the overall shape and details of generated images are respectively reconstructed in the early and final stages of it.

2. For the working mechanism of text prompt, we empirically show the special token [EOS] dominates the influence of text prompt in the early (overall shape reconstruction) stage of denoising process, when the information from text prompt is also conveyed. Subsequently, the model works on filling the details of generated images mainly depending on themselves.

3. We apply our observation to accelerate the sampling of denoising process 25%+.

2 Related Work

Diffusion Model. In this paper, our exploration is based on the Stable Diffusion [32], which now terms to be a standard T2I generation technique based on DPM [12, 36], and has been applied into various computer vision domains e.g., 3D [29, 33, 19] and video generation [26, 4]. In practice, the goal of T2I is generating an image that is consistent with a given text injected into the cross-attention module [42] of the image decoder. Therefore, understanding the working mechanism of stable diffusion potentially improves the existing techniques [1]. Unfortunately, to the best of our knowledge, the problem is limited explored, expected in [46, 35], where they similarly observe the low-frequency signals are firstly recovered in the denoising process. However, further explanations for this phenomenon are neglected in these works.

[†][EOS] contains the overall information in text prompt due to the auto-regressive CLIP text-encoder

2

Influence of Tokens. Understanding the working mechanism of encoded (by a pretrained language model) text prompt [3, 30, 43, 27] helps us understanding T2I generation [38, 16, 21]. For example, [45] finds that in LLM, the first token primarily decides the weights in the cross-attention map, which similarly appeared in the cross-modality text-image stable diffusion model as we observed. [48] explores the influence of individual tokens in counterfactual memorization. However, in the multi-modality models e.g., [30, 18, 17, 23], whereas the textual information interacted with the image in the cross-attention module as in stable diffusion, the working mechanism of tokens interacts with cross-modality data is limited explored, expected in [1]. They find in a single case that the influence of text prompts may decrease during the denoising process, while they do not proceed to study or apply this phenomenon as in this paper. Recently, [49] finds that the cross-attention map between the text prompt and generated images converges during the denoising process, which is also explained by our observations that the information conveyed during the first few denoising steps. Besides that, unlike ours, their observations are lack of theoretical explanation.

3 Preliminaries

We briefly introduce the (latent) stable diffusion model [31], which transfers a standard Gaussian noise into a target image latent that aligns with pre-given text prompts. Here, the generated data space is a low-dimensional Vector-Quantized (VQ) [7] image latent to reduce the computational cost of generation. One may get the target natural image by decoding the generated image latent. In this paper, the original data (image latent) is denoted by x_0, and the encoded textual prompt (by CLIP text encoder [30]) is represented by $\mathcal{C}$. The noisy data

$$x_t = \sqrt{\bar{\alpha}_t}x_0 + \sqrt{1 - \bar{\alpha}_t}\epsilon_t, \tag{1}$$

is used as input to diffusion model ϵ_θ trained by

$$\min_\theta \mathbb{E}\left[\|\epsilon_\theta(t, x_t, \mathcal{C}, \emptyset) - \epsilon_t\|^2\right], \tag{2}$$

with $0 \leq t \leq T$, $\epsilon_t \sim \mathcal{N}(0, I)$ independent of x_0, $\bar{\alpha}_t \to 0$ (resp. $\bar{\alpha}_t \to 1$) for $t \to 0$ (resp. $t \to T$). Here, the noise prediction model $\epsilon_\theta(t, x_t, \mathcal{C}, \emptyset)$ is constructed by classifier-free guidance [13] with

$$\epsilon_\theta(t, x_t, \mathcal{C}, \emptyset) = \epsilon_\theta(t, x_t, \emptyset) + w\left(\epsilon_\theta(t, x_t, \mathcal{C}) - \epsilon_\theta(t, x_t, \emptyset)\right), \tag{3}$$

where $\epsilon_\theta(t, x_t, \emptyset)$ is an unconditional generative model, and the $w \geq 0$ is guidance scale. As the model is trained to predict noise ϵ_t in x_t, and x_T approximates a standard Gaussian, we can conduct the reverse denoising process (DDIM [36]) transfers a standard Gaussian to target image x_0

$$x_{t-1} = \sqrt{\frac{\bar{\alpha}_{t-1}}{\bar{\alpha}_t}}x_t + \left(\sqrt{\frac{1 - \bar{\alpha}_{t-1}}{\bar{\alpha}_{t-1}}} - \sqrt{\frac{1 - \bar{\alpha}_t}{\bar{\alpha}_t}}\right)\epsilon_\theta(t, x_t, \mathcal{C}, \emptyset). \tag{4}$$

Finally, the diffusion model (usually UNet) takes the text prompt as input to the cross-attention module in each basic block [†] of diffusion model with output $\text{Attention}(Q, K, V) = \text{Softmax}(QK^\top/\sqrt{d})V$ (d is dimension of image feature), where $\phi(x_t)$ is the feature of image, and

$$Q = W_Q\phi(x_t); K = W_K\mathcal{C}; V = W_V\mathcal{C}. \tag{5}$$

4 First Overall Shape then Details

In this section, we first explore the image reconstruction process of the stable diffusion model. As noted in [1], the generated image's overall shape is difficult to be altered in the final stage of the denoising process. Inspired by this observation, and note that the low-frequency and high-frequency signals of image determine its overall shape and details, respectively [9]. We theoretically and empirically verify that the denoising process recovers the low and high-frequency signals in its initial and final stages, respectively, which explains the phenomenon of *"first overall shape then details"*.

4.1 Two Stages of Denoising Process

Settings (PromptSet**).** As in [14], we use 1600 prompts following the template "a {attribute} {noun}", with the attribute as an adjective of color or texture. We create 800 text prompts respectively

---

[†]The model is stacked by such basic blocks sequentially with residual module, self-attention module, and cross-attention module in each of it.

3

Generate Image

Text Prompt: The square coaster was next to the circular mug.

(a) Cross-Attention Map

(b) Convergence of Cross-Attention Map
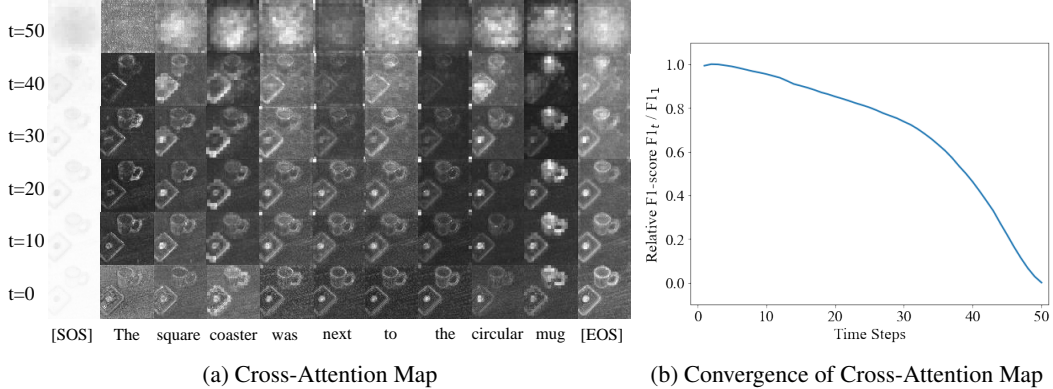
Figure 1: Figure 1a is the averaged cross-attention over denoising steps. The two generated images are on the top, and the weights in cross-attention maps of each tokens are on the bottom with whiter pixels correspond to larger weights in cross-attention map. Figure 1b is obtained by taking average over tokens and prompts in `PromptSet`, which compares the shapes of cross-attention map and final generated images, Measured by relative F1-score $\mathrm{F1}_t/\mathrm{F1}_1$ over different denoising steps.

under each of the two categories of attributes. Besides that, we add another extra 1000 complex natural prompts in [14] without a predefined sentence template. These prompts consist of the text prompts set (abbrev `PromptSet`) we used. The classes of nouns, colors, and textures are respectively 230, 33, and 23 in these prompts. In this paper, we generate images under `PromptSet` by Stable Diffusion v1.5-Base [31]. Finally, without specification, we use 50 steps DDIM sampling [36].

From [40], though stable diffusion generates encoded VQ image latents [7]. These latents preserve semantic information transformed by text prompt through cross-attention module (5). Notably, in the cross-attention module, the pixel is a weighted sum of token embedding with cross-attention map $\mathrm{Softmax}(QK^\top/\sqrt{d})$ as weights. The weights reveal the semantic information of token, as they are the correlations between image query Q and textual key K. To check the correlation, we visualize the averaged cross-attention map over all layers of model $\epsilon_{\boldsymbol{\theta}}$ under different time steps t, from 50 to 1.

Interestingly, the cross-attention map of each token already has a semantic shape in the early stage of the denoising process, e.g., for $t = 40$ in example Figure 1a. This can hold only if the overall shape of the image is constructed in this early stage, so that each pixel can correspond to the correct token. To further investigate this, we compute the average cross-attention map of each token under the aforementioned `PromptSet`. We compare the shape of the cross-attention map and the final generated image quantitatively by transforming them into canny images [9] and computing the F1-score [39] ($\mathrm{F1}_t$ for each t) between these canny images. To compare the difference over different time steps more clearly, we plot the relative F1-score $\mathrm{F1}_t/\mathrm{F1}_1$ ($t = 1$ the image has been recovered). The result in Figure 1b shows the shape of the cross-attention map rapidly close to the ones of the generated image in the early stage of denoising, which is consistent with our speculation and the result in [49], where they conclude that the cross-attention map will converge during the denoising process.

4.2 Frequency Analysis

To further explain the above phenomenon, we refer to the frequency-signal analysis. It has been well explored that the low-frequency signals represent the overall smooth areas or slowly varying components of an image (related to the overall shape). On the other hand, the high-frequency signals correspond to the fine details or rapid changes in intensity (related to attributes like textures) [9]. Thereafter, to explain the "first overall shape then details" in the denoising process, it is natural to refer to the variations in frequency signals of images during the denoising process.

Mathematically, suppose the clean data (image latent) $\boldsymbol{x}_0$ has $M \times N$ dimensions for each channel with $\boldsymbol{x}_t$ defined in (1). Then the Fourier transformation $F_{\boldsymbol{x}_t}(u, v)$ (with $u \in [M], v \in [N]$) of $\boldsymbol{x}_t$ is

$$
\begin{aligned}
F_{\boldsymbol{x}_t}(u, v) &= \frac{1}{MN} \sum_{k=0}^{M-1} \sum_{l=0}^{N-1} \boldsymbol{x}_t^{kl} \exp\left(-2\pi\mathrm{i}\left(\frac{ku}{M} + \frac{lv}{N}\right)\right) \\
&= \sqrt{\bar{\alpha}_t} F_{\boldsymbol{x}_0}(u, v) + \sqrt{1 - \bar{\alpha}_t} F_{\boldsymbol{\epsilon}_t}(u, v),
\end{aligned}
\tag{6}
$$

4
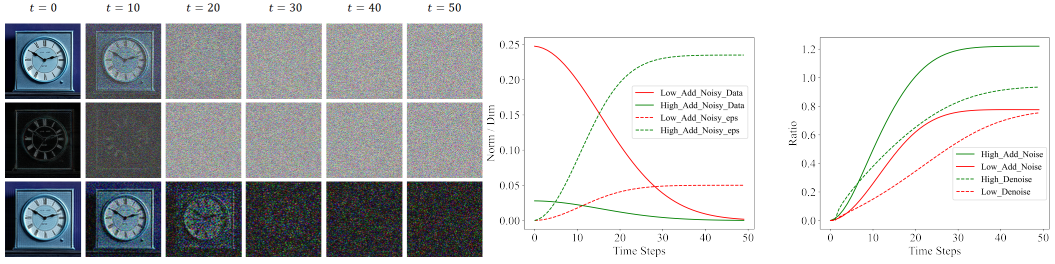
(a) Noisy data and its high, low frequency parts

(b) Norm of features $\sqrt{\bar{\alpha}_t}\boldsymbol{x}_0$ and $\sqrt{1-\bar{\alpha}_t}\boldsymbol{\epsilon}_t$

(c) Ratio of high / low frequency parts variation

Figure 2: Figure 2a visualizes the completed noisy data and its high-frequency, and low-frequency parts over different time steps, listed from top to bottom. Figures 2b and 2c measure the low/high-frequency signals of $\boldsymbol{x}_t$. In Figure 2b, "Low_Add_Noisy_Data/eps" means the norm of $\sqrt{\bar{\alpha}_t}\boldsymbol{x}_0^{\text{low}}$ and $\sqrt{1-\bar{\alpha}_t}\boldsymbol{\epsilon}_t^{\text{low}}$, vise versa for "High_...". On the other hand, Figure 2c measures the variation ratio of high/low frequency parts of images during the noising/denoising process. For example, "High_Add_Noise" represents $\|\boldsymbol{x}_t^{\text{high}} - \boldsymbol{x}_0^{\text{high}}\|/\|\boldsymbol{x}_0^{\text{high}}\|$ during noising process.

where $\sqrt{-1} = \text{i}$, and $\boldsymbol{x}_t^{kl}$ is the (k,l) component of $\boldsymbol{x}_t$. As we do not now the distribution of $\boldsymbol{x}_0$, we explore the $F_{\boldsymbol{\epsilon}_t}(u,v)$ in sequel. The result is in the following proposition proved in Appendix A.

Proposition 1. *For all $u \in [M], v \in [N]$, with high probability, the complex number $F_{\boldsymbol{\epsilon}_t}(u,v)$ satisfies*

$$\|F_{\boldsymbol{\epsilon}_t}(u,v)\|^2 \approx \mathcal{O}\left(\frac{1}{MN}\right). \tag{7}$$

This proposition indicates that under large image size (MN), the strength of frequency signals (no matter low or high) of standard Gaussian are equally close to zero. Thus, the frequency signal of $\boldsymbol{x}_0$ in noisy data $\boldsymbol{x}_t$ is mainly corrupted by the shrink factor $\bar{\alpha}_t$ due to (6), instead of the noise in it.

However, as visualized in Figure 2a [†], in contrast to high-frequency part of image, the image's low-frequency parts [†] are more robust than the ones of high-frequency. For example, for $t = 20$ in Figure 2a, the shape of the clock is still perceptible in the low-frequency part of the image. [†] If this fact is generalized to image latent, then it explains the two stages of generation as observed in Section 4.1. Because the low-frequency parts are not corrupted until the end of the adding noise process. Then, it will be recovered at the beginning of the reverse denoising process.

To investigate this, in Figures 2b and 2c, we plot the averaged results over time steps of variation of low/high-frequency parts in images generated by PromptSet. In these figures, $\boldsymbol{x}_t^{\text{low}}$ is the low-frequency part of $\boldsymbol{x}_t$ and vice-versa for high-frequency part $\boldsymbol{x}_t^{\text{high}}$. As can be seen, in Figure 2c, the behavior of $\boldsymbol{x}_t$ is similar under add/de noise processes, and the reconstruction of low-frequency signals is faster than the high-frequency signals. On the other hand, by comparing "Low_..._Data" ($\|\sqrt{\bar{\alpha}_t}\boldsymbol{x}_0^{\text{low}}\|$) and "High_..._Data" ($\|\sqrt{\bar{\alpha}_t}\boldsymbol{x}_0^{\text{high}}\|$) in Figure 2b, we observe the strength of high-frequency signals are significantly lower than the low-frequency signals, which seems to be a property adopted from natural image [9]. However, the relationship oppositely holds for Gaussian noise, which is implied by Proposition 1, as the frequency signals of noise $\boldsymbol{\epsilon}_t$ under each spectrum are all close to zero, while the high-frequency parts contain 80% spectrum, so that $\boldsymbol{\epsilon}_t^{\text{high}}$ is larger than the $\boldsymbol{\epsilon}_t^{\text{low}}$.

These observations explain the phenomenon "first overall shape then details". Since the low-frequency parts of the image (decide overall shape) are not totally corrupted until the end of the noising process. Thus, they will be firstly recovered during the reverse denoising process, while the phenomenon does not hold for low-frequency parts of the image, as they are quickly corrupted during the noising process, so they will not be recovered until the end of denoising.

[†]Please note that the t in Figure 2a and the other parts of this paper refers to the corresponding t-th time step of 50-steps DDIM sampling, which corresponds to $20t$ steps in [12]

[†]We distinguish low frequency by threshold 20%, i.e., the lowest 20% parts of spectrum are low-frequency.

[†]This fact is also observed in [35, 46], while they leverage this phenomenon to refine the architecture of UNet, and the rationale behind the phenomenon is unexplored.

5
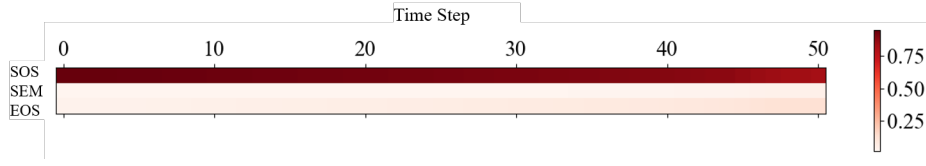
Figure 3: Averaged weights in cross-attention map over pixels of three classes of tokens. For each prompt in `PromptSet`, the result is obtained by taking average over tokens in each class. The final result is the average over `PromptSet`. Notably, the weights on [SOS] are all larger than 0.9.
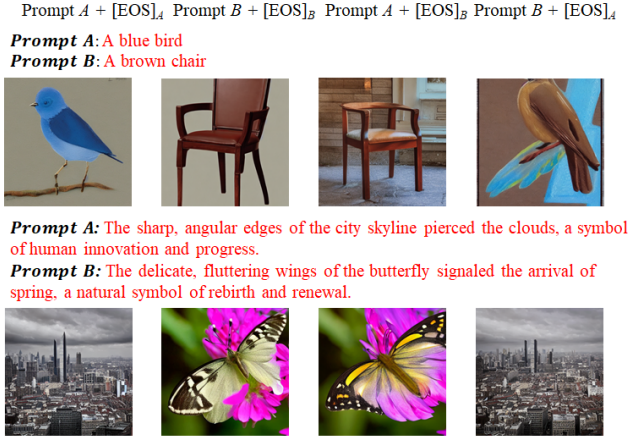
Figure 4: Images under prompts from `S-PromptSet` with switched [EOS]. The objects are consistent with the ones conveyed by [EOS], while some information in semantic tokens is still conveyed.

5 The Working Mechanism of Text Prompt

We have verified that the denoising process has two stages i.e., "first overall shape then details". Next, we explore the working mechanism of text prompts during these stages. Our main observations are two fold, 1): The special tokens [EOS] dominate the influence of text prompt. 2): The text prompt mainly works on the first overall shape reconstruction stage of the denoising process.

5.1 [EOS] Contains More Information

In T2I diffusion, the text prompt is encoded by auto-regressive CLIP text encoder, with semantic tokens (SEM) enclosed with special tokes [SOS] and [EOS]. For such three classes of tokens, as the information in these tokens is conveyed by the cross-attention module, we first compute the averaged weights over pixels in the cross-attention map for each class. The weights are computed by taking the average over `PromptSet` and presented in Figure 3. As can be seen, the weights of [SOS] are significantly larger than the other classes. However, due to the CLIP text encoder is an auto-regressive model, [SOS] does not contain any semantic information. Therefore, we conclude that the influence of [SOS] is mainly adjusting the whole cross-attention map i.e., weights on the other tokens. To further verify this conclusion, we conduct experiments in Appendix I.1. A similar phenomenon is observed in single-modality LLM [45]. As the information of text prompt is conveyed by semantic tokens and [EOS], we will focus on them instead of [SOS] in the sequel.

As both SEM and [EOS] contain the semantic information in the text prompt, we first explore which of them has larger impact on T2I generation. To this end, we select 3000 pairs of text prompts from `PromptSet` (2000 pairs follow the template, the other 1000 pairs have complex prompts), where the two text prompts are represented as "[SOS] + Prompt A (B) + $[EOS]_{A(B)}$". For each pair, we switch their [EOS] to construct the new text prompt pairs as "[SOS] + Prompt A (B) + $[EOS]_{B(A)}$".

We examine the generated images under these artificially constructed text prompts (namely `Switched-PromptSet` (`S-PromptSet`)). We call A from Prompt$_A$ as "source" and B from $[EOS]_B$ as "target" for "[SOS] + Prompt A + $[EOS]_B$", and vice versa. For the generated images under these prompts, we measure their alignments with the source and target prompts, respectively. The used metrics are the three standard ones in measuring text-image alignment: CLIPScore [30, 10], BLIP-VQA [18, 14], and MiniGPT4-CoT [51, 14] (details are in Appendix B).

The results are in Table 1. Surprisingly, the generated images under the constructed text prompts are more likely to be aligned with the target prompt instead of the source prompt. That says, even

6

A: Source; B: Target   move of **start step** a switches [EOS]

$t = T$ $t = a$ $t = 0$

$t \in [a, T]$: Prompt A + [EOS]$_B$ $t \in [0, a]$: Prompt A + [EOS]$_A$
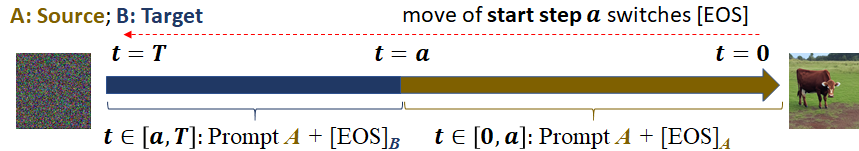
Figure 5: Desnoising process under text prompt with switched [EOS] in $[a, 50]$.

Table 1: The alignment of generated image with its source and target prompts. The prompts are constructed with switched [EOS].

Prompt Alignment	Source	Target
Text-CLIPScore ↑	0.2363	**0.2758**
BLIP-VQA↑	0.3325	**0.4441**
MiniGPT-CoT↑	0.6473	**0.7213**
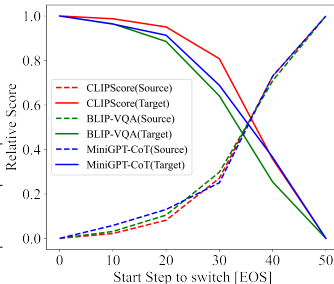
Figure 6: Relative text-image alignments ("current minus worst" over "best minus worst") with source (or target) prompt under switched [EOS] (substitution in [Start Step, 50], Figure 5). Alignments with source and target prompts are respectively solid and dot lines.

with prefixed irrelevant semantic tokens, the information contained in [EOS] dominates the denoising process (especially for overall shape) as in Figure 4. Thus, we conclude that the special tokens [EOS] have a larger impact than semantic tokens in prompt during T2I generation. We have two speculations about this phenomenon. 1): Owing to the auto-regressive encoded text prompt, unlike semantic tokens, [EOS] contains complete textual information, so that it decides the pattern of the generated image. 2): The number of [EOS] is usually larger than semantic tokens, as the prompt is enclosed by [EOS] to length 76. An ablation study in Appendix C verifies this speculation.

In summary, our conclusion in this subsection can be summarized as: ***In T2I generation, the special token [EOS] decides the overall information (especially shape) of the generated image.***

Remark 1. *For the generated images under S-PromptSet, we find some information in semantic tokens is also conveyed, especially for the attribute information in it, e.g., "brown" color in the last image of the first row in Figure 4. We explore this in Appendix D and explain this as: unlike noun information, attributes in semantic tokens may not conflict with the contained information in [EOS] (which quickly decides the overall shape of the generated image), so that has potential to be conveyed.*

5.2 The Text Prompt Mainly Working on the First Stage

In Section 4.1, we have conclude that the denoising process is divided into two stages "first overall shape then details". Next, we explore the relationships between text prompts and the two stages. We start with special tokens [EOS] which contain major information in T2I generation. During the whole 50 denoising steps of T2I generation under prompts from S-PromptSet, we vary the starting point of substituting [EOS] i.e., the used text prompt is "[SOS] + Prompt A + [EOS]$_B$ (resp. [EOS]$_A$) for $t \in [\text{Start Step}, 50]$ (resp. $t \in [0, \text{Start Step}]$) with "Start Step" $\in [0, 50]$, i.e., Figure 5. We compare the alignments of generated images with source / target prompts as in Figure 6.

In Figure 6, the alignment with the target prompt slightly decreases, until the "Start Step" of substitution close to 50. This shows that the information in [EOS] has been conveyed during the first few steps of the denoising, which is the overall shape reconstruction stage according to Section 4.

Following the revealed working stage of [EOS], we explore whether the whole text prompt also works in this stage. If so, the T2I generation will only depends on $\epsilon_{\theta}(t, \boldsymbol{x}_t, \emptyset)$ in (3) for small t. To see this, we vary the w in (3) to control the injected information from the text prompt during the denoising process. Concretely, for a as the starting step of removing text prompt, i.e., during $t \in [0, a)$, we use $w = 7.5$, and $w = 0$ for $t \in [a, 50]$, where $a \in [0, 50]$. Then, the text prompt only works for $t \in [0, a)$. We generate target images $\boldsymbol{x}_0^{50}$ under PromptSet with standard denoising process ($a = 50$), and compare them with the ones $\boldsymbol{x}_0^a$ generated under varied $a \in [0, 50]$ (Figure 7). The image-image alignments are measured by standard metrics CLIPScore and L_1-distance [9]. To eliminate magnitude, we report relative results, i.e., "current minus worst" over "best minus worst".

The results are in Figure 8a. During generation, the text information is absence for $t \in [a, 50]$, while Figure 8a indicates that alignments between $\boldsymbol{x}_0^a$ and target $\boldsymbol{x}_0^{50}$ will quickly be small only for large a (from 30 to 50). This shows that only if removing the textual information under large t, its influence to generated image is removed. Therefore, we can conclude: ***The information of text prompt is***

7
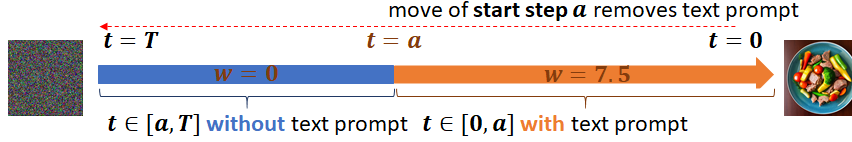
Figure 7: Desnoising with text prompt injected in $[0, a]$.

(a) Relative Image-Alignment

(b) Norm/Dim of (Un)/Conditional Model
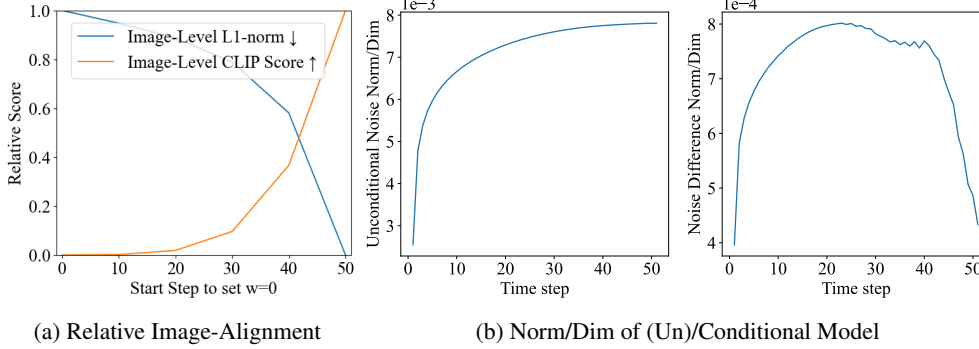
Figure 8: Figure 8a is the relative difference "current minus worst" over "best minus worst" under different start step a of Denoising process Figure 7. The last two figures 8b are per-dimensional norm of unconditional noise $\epsilon_{\theta}(t, x_t, \emptyset)$ and noise difference $w\left(\epsilon_{\theta}(t, x_t, \mathcal{C}) - \epsilon_{\theta}(t, x_t, \emptyset)\right)$

conveyed during the early stage of denoising process. Therefore, the overall shape of generated image is mainly decided by the text prompt, while the its details are then reconstructed by itself.

Discussion. Next, let us explain the phenomenon. Technically, in (3), the $\epsilon_{\theta}(t, x_t, \mathcal{C}, \emptyset)$ was proposed to approximate $\nabla_{x} \log p_t(x_t \mid \mathcal{C})/\sqrt{1 - \bar{\alpha}_t}$ with decomposition (p_t is the density of x_t)

$$\nabla_{x} \log p_t(x_t \mid \mathcal{C}) = \nabla_{x} \log p_t(x_t) + \nabla_{x} \log p_t(\mathcal{C} \mid x_t). \tag{8}$$

Comparing (3) and (8), it holds $\epsilon_{\theta}(t, x_t, \emptyset) \propto \nabla_{x} \log p_t(x_t)^{\dagger}$ and $w(\epsilon_{\theta}(t, x_t, \mathcal{C})x - \epsilon_{\theta}(t, x_t, \emptyset)) \propto \nabla \log p_t(\mathcal{C} \mid x_t)$. From [37], the denoising process (4) aims to maximize log-likelihood $\log p_0(x_0 \mid \mathcal{C})$. Then, moving along the direction $\nabla_{x} \log p_t(\mathcal{C} \mid x_t)$ (leads to large $\log p_t(\mathcal{C} \mid x_t)$) push x_t to be aligned with the text prompt $\mathcal{C}$ during the decreasing of t. Adding such a moving direction is standard in conditional generation [25, 36, 8, 24]. As shown in Figure 8b, during the denoising process, x_t will gradually to be consistent with $\mathcal{C}$, so that $\nabla \log p_t(\mathcal{C} \mid x_t)$ will decrease with t. Thereafter, we observe the impact of text prompt conveyed by this term decreases with $t \to 0$. Notably, owing to the quickly reconstructed overall shape of image in Section 4, the generated x_t will quickly be consistent with $\mathcal{C}$, so that explain the quickly decreasing $\nabla \log p_t(\mathcal{C} \mid x_t)$.

Remark 2. *In this section, we verify the injected textual information are all conveyed in the first stage of diffusion process. In fact, this phenomenon is also generalized to the other types of information, e.g., conditional image information in subject-driven generation [44, 50], we verify this in Appendix H.*

6 Application

Acceleration of Sampling. Since the information contained in text prompt is mainly conveyed by the noise prediction with condition $\epsilon_{\theta}(t, x_t, \mathcal{C})$, we can consider removing the evaluation of after the first few steps of denoising process. This is because the information in text prompt has been conveyed in this stage, and the computational cost can be significantly reduced without evaluating $\epsilon_{\theta}(t, x_t, \mathcal{C})$.

Therefore, we substitute the noise prediction $\epsilon_{\theta}(t, x_t, \mathcal{C}, \emptyset)$ as

$$\epsilon_{\theta}(t, x_t, \mathcal{C}, \emptyset) = \begin{cases} \epsilon_{\theta}(t, x_t, \emptyset) + w\left(\epsilon_{\theta}(t, x_t, \mathcal{C}) - \epsilon_{\theta}(t, x_t, \emptyset)\right) & a \leq t; \\ \epsilon_{\theta}(t, x_t, \emptyset) & 0 \leq t < a. \end{cases} \tag{9}$$

---

†This can be verified by the training strategy of it in [31], where $\epsilon_{\theta}(t, x_t, \emptyset)$ is used to predict noise in noisy data without condition injected.

8

move of **start step a** adds text prompt

$t = T$ $t = a$ $t = 0$

$w = 7.5$ $w = 0$

$t \in [a, T]$ **with** text prompt $t \in [0, a]$ **without** text prompt
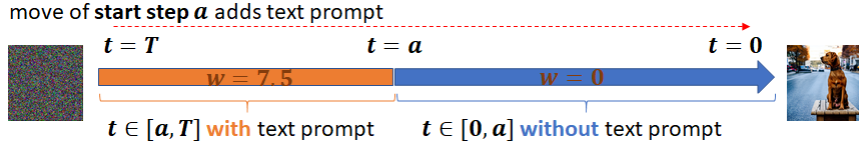
Figure 9: Desnoising under ϵ_θ (9). The text prompt is injected in $[a, T]$, instead of $[0, a]$ in Figure 7.

Start point $a = 0$ (baseline) $a = 5$ $a = 10$ $a = 15$ $a = 20$ $a = 25$ w/o text

A dog standing on a bench during the day.

SD v1.5

SD v2.1

Pixart-Alpha
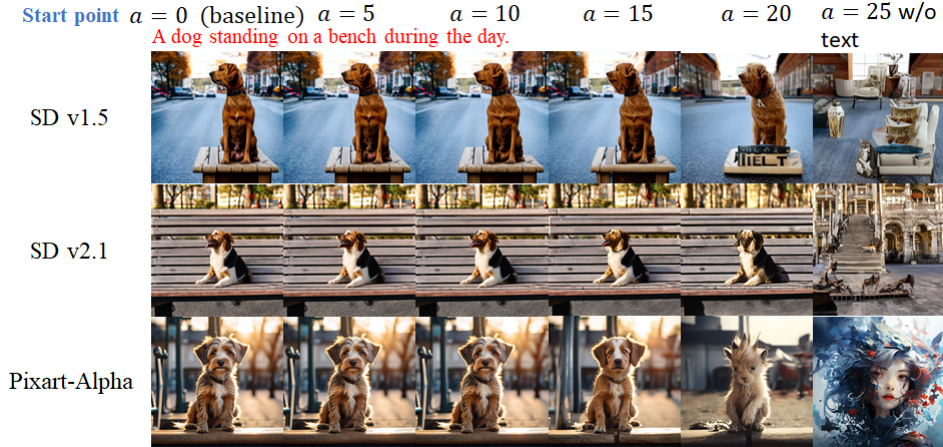
Figure 10: The generated images with 25 steps DPM-Solver under ϵ_θ in (9) (Figure 9). The textual information is removed during $t \in [0, a]$. With $a \to 25$, the inference cost is decreased.

Table 2: The difference between images generated under varied a with the ones of $a = 0$. The results are averaged over 30K generated images, and saved latency is evaluated on one V100 GPU.

Start point a	0 (baseline)	10	20	30	40	50	0 (baseline)	5	10	15	20	25
Sampler / Backbone			DDIM / SD v1.5						DPM-Solver / SD v1.5			
Image-CLIPScore ↑	1.000	0.998	0.996	0.971	0.838	0.539	1.000	0.999	0.994	0.956	0.798	0.533
L_1-distance ↓	0.000	0.011	0.022	0.043	0.087	0.195	0.000	0.015	0.027	0.050	0.100	0.188
Saved Latency ↑	0.00%	7.84%	18.10%	27.18%	35.24%	48.47%	0.00%	8.36%	17.95%	26.11%	34.86%	47.60%
FID ↓	13.772	13.770	13.805	14.012	15.048	19.296	14.297	14.286	14.725	14.985	15.860	19.758
Text-CLIPScore ↑	31.040	31.001	30.894	30.493	28.172	16.682	30.992	30.891	30.772	30.205	26.843	16.721
Sampler / Backbone			DDIM / SD v2.1						DPM-Solver / SD v2.1			
Image-CLIPScore ↑	1.000	0.999	0.998	0.986	0.902	0.550	1.000	0.999	0.998	0.988	0.901	0.543
L_1-distance ↓	0.000	0.017	0.041	0.077	0.152	0.386	0.000	0.026	0.046	0.083	0.160	0.369
Saved Latency ↑	0.00%	8.68%	18.95%	28.16%	36.19%	47.99%	0.00%	8.75%	18.28%	26.24%	35.48%	47.75%
FID ↓	13.014	13.011	13.046	13.247	14.242	18.472	13.507	13.500	13.914	14.159	15.015	18.983
Text-CLIPScore ↑	31.413	31.405	31.362	31.113	29.717	16.706	31.339	31.326	31.292	31.045	29.653	16.639
Sampler / Backbone			DDIM / Pixart-Alpha						DPM-Solver / Pixart-Alpha			
Image-CLIPScore ↑	1.000	0.999	0.935	0.744	0.643	0.522	1.000	0.999	0.993	0.911	0.648	0.625
L_1-distance ↓	0.000	0.024	0.058	0.103	0.169	0.247	0.000	0.013	0.022	0.046	0.098	0.199
Saved Latency ↑	0.00%	8.24%	17.98%	27.20%	34.95%	49.15%	0.00%	7.92%	15.77%	25.18%	33.80%	48.10%
FID ↓	22.651	22.884	23.258	25.485	29.760	36.525	18.669	18.520	18.798	19.358	20.494	26.159
Text-CLIPScore ↑	28.157	27.979	25.719	19.640	14.986	14.586	30.733	30.721	30.745	29.416	20.629	14.928

By varying $a \to T$ in (9), the inference cost is reduced as an evaluation of $\epsilon_\theta(t, \boldsymbol{x}_t, \mathcal{C})$ is saved.

To evaluate the saved computational cost of using noise prediction (9) during inference and the quality of generated data, we consider applying it on two standard samplers DDIM [36] and DPM-Solver [22] on a benchmark dataset MS-COCO [20] in T2I generation. We consider backbone models Stable-Diffusion (SD) v1.5-Base, SD v2.1-Base [31], and Pixart-Alpha [5]. Concretely, we apply noise prediction (9) with varied a to generate 30K images from 30K text prompts in the test set of MS-COCO, for each sampler and backbone model. We compare the difference (measured by L_1-distance and Image-Level CLIPScore) between the generated images under $a > 0$ and $a = 0$ (the standard noise prediction). The results are in Table 2, where we also report the Frechet Inception Distance (FID) score [11] under each a to evaluate the quality of generated images.

The Table 2 indicates that proper a in (9) significantly reduces the computation cost during the inference stage without deteriorate the quality of generated images. For example, SD v1.5 with $a = 20$ saves 27+% computational cost, but generates images close to the baseline method ($a = 0$).

9

7 Conclusion

In this paper, we investigate the working mechanism of T2I diffusion model. By empirical and theoretical (frequency) analysis, we conclude that the denoising process firstly constructs the overall shape then details of the generated image. Next, we explore the working mechanism of text prompts. We find its special token `[EOS]` has a significant impact on the overall shape in the first stage of the denoising process, in which the information in the text prompt is conveyed. Then, the details of images are mainly reconstructed by themselves in the latter stage of generation. Finally, we apply our conclusion to accelerate the inference of T2I generation, and save 25%+ computational cost.

Acknowledgement

We gratefully acknowledge the support of Mindspore, CANN(Compute Architecture for Neural Networks) and Ascend AI Processor used for this research.

References

[1] Yogesh Balaji, Seungjun Nah, Xun Huang, Arash Vahdat, Jiaming Song, Karsten Kreis, Miika Aittala, Timo Aila, Samuli Laine, Bryan Catanzaro, et al. ediffi: Text-to-image diffusion models with an ensemble of expert denoisers. Preprint arXiv:2211.01324, 2022.

[2] Fan Bao, Shen Nie, Kaiwen Xue, Yue Cao, Chongxuan Li, Hang Su, and Jun Zhu. All are worth words: A vit backbone for diffusion models. In *Conference on Computer Vision and Pattern Recognition*, 2023.

[3] Tom Brown, Benjamin Mann, Nick Ryder, Melanie Subbiah, Jared D Kaplan, Prafulla Dhariwal, Arvind Neelakantan, Pranav Shyam, Girish Sastry, Amanda Askell, et al. Language models are few-shot learners. 2020.

[4] Wenhao Chai, Xun Guo, Gaoang Wang, and Yan Lu. Stablevideo: Text-driven consistency-aware diffusion video editing. In *International Conference on Computer Vision*, 2023.

[5] Junsong Chen, YU Jincheng, GE Chongjian, Lewei Yao, Enze Xie, Zhongdao Wang, James Kwok, Ping Luo, Huchuan Lu, and Zhenguo Li. Pixart-alpha: Fast training of diffusion transformer for photorealistic text-to-image synthesis. In *International Conference on Learning Representations*, 2024.

[6] Florinel-Alin Croitoru, Vlad Hondru, Radu Tudor Ionescu, and Mubarak Shah. Diffusion models in vision: A survey. *IEEE Transactions on Pattern Analysis and Machine Intelligence*, 2023.

[7] Patrick Esser, Robin Rombach, and Bjorn Ommer. Taming transformers for high-resolution image synthesis. In *Conference on Computer Vision and Pattern Recognition*, 2021.

[8] Karim Farid, Simon Schrodi, Max Argus, and Thomas Brox. Latent diffusion counterfactual explanations. Preprint arXiv:2310.06668, 2023.

[9] Rafael C Gonzales and Paul Wintz. *Digital image processing*. Addison-Wesley Longman Publishing Co., Inc., 1987.

[10] Jack Hessel, Ari Holtzman, Maxwell Forbes, Ronan Le Bras, and Yejin Choi. Clipscore: A reference-free evaluation metric for image captioning. In *Conference on Empirical Methods in Natural Language Processing*, 2021.

[11] Martin Heusel, Hubert Ramsauer, Thomas Unterthiner, Bernhard Nessler, and Sepp Hochreiter. Gans trained by a two time-scale update rule converge to a local nash equilibrium. 2017.

[12] Jonathan Ho, Ajay Jain, and Pieter Abbeel. Denoising diffusion probabilistic models. In *Advances in Neural Information Processing Systems*, 2020.

[13] Jonathan Ho and Tim Salimans. Classifier-free diffusion guidance. In *NeurIPS 2021 Workshop on Deep Generative Models and Downstream Applications*, 2021.

10

[14] Kaiyi Huang, Kaiyue Sun, Enze Xie, Zhenguo Li, and Xihui Liu. T2i-compbench: A comprehensive benchmark for open-world compositional text-to-image generation. In *Conference on Neural Information Processing Systems Datasets and Benchmarks Track*, 2023.

[15] Minguk Kang, Jun-Yan Zhu, Richard Zhang, Jaesik Park, Eli Shechtman, Sylvain Paris, and Taesung Park. Scaling up gans for text-to-image synthesis. In *Conference on Computer Vision and Pattern Recognition*, 2023.

[16] Kalpesh Krishna, Yapei Chang, John Wieting, and Mohit Iyyer. Rankgen: Improving text generation with large ranking models. In *Empirical Methods in Natural Language Processing*, 2022.

[17] Junnan Li, Dongxu Li, Silvio Savarese, and Steven Hoi. Blip-2: Bootstrapping language-image pre-training with frozen image encoders and large language models. Preprint arXiv:2301.12597, 2023.

[18] Junnan Li, Dongxu Li, Caiming Xiong, and Steven Hoi. Blip: Bootstrapping language-image pre-training for unified vision-language understanding and generation. In *International Conference on Machine Learning*, 2022.

[19] Chen-Hsuan Lin, Jun Gao, Luming Tang, Towaki Takikawa, Xiaohui Zeng, Xun Huang, Karsten Kreis, Sanja Fidler, Ming-Yu Liu, and Tsung-Yi Lin. Magic3d: High-resolution text-to-3d content creation. In *Conference on Computer Vision and Pattern Recognition*, 2023.

[20] Tsung-Yi Lin, Michael Maire, Serge Belongie, James Hays, Pietro Perona, Deva Ramanan, Piotr Dollár, and C Lawrence Zitnick. Microsoft coco: Common objects in context. In *European Conference on Computer Vision*, 2014.

[21] Nelson F Liu, Kevin Lin, John Hewitt, Ashwin Paranjape, Michele Bevilacqua, Fabio Petroni, and Percy Liang. Lost in the middle: How language models use long contexts. Preprint arXiv:2307.03172, 2023.

[22] Cheng Lu, Yuhao Zhou, Fan Bao, Jianfei Chen, Chongxuan Li, and Jun Zhu. Dpm-solver: A fast ode solver for diffusion probabilistic model sampling in around 10 steps. In *Advances in Neural Information Processing Systems*, 2022.

[23] Timo Lüddecke and Alexander Ecker. Image segmentation using text and image prompts. In *Conference on Computer Vision and Pattern Recognition*, 2022.

[24] Nishtha Madaan, Inkit Padhi, Naveen Panwar, and Diptikalyan Saha. Generate your counterfactuals: Towards controlled counterfactual generation for text. In *Association for the Advancement of Artificial Intelligence*, 2021.

[25] Petr Marek, Vishal Ishwar Naik, Anuj Goyal, and Vincent Auvray. Oodgan: Generative adversarial network for out-of-domain data generation. In *Conference of the North American Chapter of the Association for Computational Linguistics*, 2021.

[26] Eyal Molad, Eliahu Horwitz, Dani Valevski, Alex Rav Acha, Yossi Matias, Yael Pritch, Yaniv Leviathan, and Yedid Hoshen. Dreamix: Video diffusion models are general video editors. Preprint arXiv:2302.01329, 2023.

[27] OpenAI. Gpt-4 technical report. Preprint arXiv:2304.10592, 2023.

[28] William Peebles and Saining Xie. Scalable diffusion models with transformers. In *International Conference on Computer Vision*, 2023.

[29] Ben Poole, Ajay Jain, Jonathan T Barron, and Ben Mildenhall. Dreamfusion: Text-to-3d using 2d diffusion. In *International Conference on Learning Representations*, 2022.

[30] Alec Radford, Jong Wook Kim, Chris Hallacy, Aditya Ramesh, Gabriel Goh, Sandhini Agarwal, Girish Sastry, Amanda Askell, Pamela Mishkin, Jack Clark, et al. Learning transferable visual models from natural language supervision. In *International conference on machine learning*, 2021.

11

[31] Aditya Ramesh, Prafulla Dhariwal, Alex Nichol, Casey Chu, and Mark Chen. Hierarchical text-conditional image generation with clip latents. Preprint arXiv:2204.06125, 2022.

[32] Robin Rombach, Andreas Blattmann, Dominik Lorenz, Patrick Esser, and Björn Ommer. High-resolution image synthesis with latent diffusion models. In *Conference on Computer Vision and Pattern Recognition*, 2022.

[33] Nataniel Ruiz, Yuanzhen Li, Varun Jampani, Yael Pritch, Michael Rubinstein, and Kfir Aberman. Dreambooth: Fine tuning text-to-image diffusion models for subject-driven generation. In *Conference on Computer Vision and Pattern Recognition*, 2023.

[34] Chitwan Saharia, William Chan, Saurabh Saxena, Lala Li, Jay Whang, Emily L Denton, Kamyar Ghasemipour, Raphael Gontijo Lopes, Burcu Karagol Ayan, Tim Salimans, et al. Photorealistic text-to-image diffusion models with deep language understanding. In *Advances in Neural Information Processing Systems*, 2022.

[35] Chenyang Si, Ziqi Huang, Yuming Jiang, and Ziwei Liu. Freeu: Free lunch in diffusion u-net. Preprint arXiv:2309.11497, 2023.

[36] Jiaming Song, Chenlin Meng, and Stefano Ermon. Denoising diffusion implicit models. In *International Conference on Learning Representations*, 2022.

[37] Yang Song, Jascha Sohl-Dickstein, Diederik P Kingma, Abhishek Kumar, Stefano Ermon, and Ben Poole. Score-based generative modeling through stochastic differential equations. In *International Conference on Learning Representations*, 2020.

[38] Simeng Sun, Kalpesh Krishna, Andrew Mattarella-Micke, and Mohit Iyyer. Do long-range language models actually use long-range context? In *Conference on Empirical Methods in Natural Language Processing*, 2021.

[39] Abdel Aziz Taha and Allan Hanbury. Metrics for evaluating 3d medical image segmentation: analysis, selection, and tool. *BMC Medical Imaging*, 15:29, 2015.

[40] Raphael Tang, Akshat Pandey, Zhiying Jiang, Gefei Yang, Karun Kumar, Jimmy Lin, and Ferhan Ture. What the daam: Interpreting stable diffusion using cross attention. 2023.

[41] Vladimir Vapnik. *The nature of statistical learning theory*. Springer science & business media, 1999.

[42] Ashish Vaswani, Noam Shazeer, Niki Parmar, Jakob Uszkoreit, Llion Jones, Aidan N Gomez, Łukasz Kaiser, and Illia Polosukhin. Attention is all you need. *Advances in Neural Information Processing Systems*, 2017.

[43] Jason Wei, Xuezhi Wang, Dale Schuurmans, Maarten Bosma, Fei Xia, Ed Chi, Quoc V Le, Denny Zhou, et al. Chain-of-thought prompting elicits reasoning in large language models. 2022.

[44] Yu Liu Yujun Shen Deli Zhao Hengshuang Zhao Xi Chen, Lianghua Huang. Anydoor: Zero-shot object-level image customization. In *Conference on Computer Vision and Pattern Recognition*, 2024.

[45] Guangxuan Xiao, Yuandong Tian, Beidi Chen, Song Han, and Mike Lewis. Efficient streaming language models with attention sinks. Preprint arXiv:2309.17453, 2023.

[46] Xingyi Yang, Daquan Zhou, Jiashi Feng, and Xinchao Wang. Diffusion probabilistic model made slim. In *Conference on Computer Vision and Pattern Recognition*, 2023.

[47] Jiahui Yu, Yuanzhong Xu, Jing Yu Koh, Thang Luong, Gunjan Baid, Zirui Wang, Vijay Vasudevan, Alexander Ku, Yinfei Yang, Burcu Karagol Ayan, et al. Scaling autoregressive models for content-rich text-to-image generation. *Transactions on Machine Learning Research*, 2022.

[48] Chiyuan Zhang, Daphne Ippolito, Katherine Lee, Matthew Jagielski, Florian Tramèr, and Nicholas Carlini. Counterfactual memorization in neural language models. Preprint arXiv:2112.12938, 2021.

12

[49] Wentian Zhang, Haozhe Liu, Jinheng Xie, Francesco Faccio, Mike Zheng Shou, and Jürgen Schmidhuber. Cross-attention makes inference cumbersome in text-to-image diffusion models. Preprint arXiv:2404.02747, 2024.

[50] Xintao Wang Zhongang Qi Ming-Ming Cheng Ying Shan Zhen Li, Mingdeng Cao. Photomaker: Customizing realistic human photos via stacked id embedding. In *Conference on Computer Vision and Pattern Recognition*, 2024.

[51] Deyao Zhu, Jun Chen, Xiaoqian Shen, Xiang Li, and Mohamed Elhoseiny. Minigpt-4: Enhancing vision-language understanding with advanced large language models. Preprint arXiv:2304.10592, 2023.

13

A Proofs of Proposition 1

Proposition 1. *For all $u \in [M], v \in [N]$, with high probability, the complex number $F_{\boldsymbol{\epsilon}_t}(u,v)$ satisfies*

$$\|F_{\boldsymbol{\epsilon}_t}(u,v)\|^2 \approx \mathcal{O}\left(\frac{1}{MN}\right). \tag{7}$$

Proof. Note that $\boldsymbol{\epsilon}_t^{kl}$ (abbreviated as $\boldsymbol{\epsilon}^{kl}$) are i.i.d. Gaussian random variable for each of k,l. Thus we have

$$F_{\boldsymbol{\epsilon}}(u,v) = \frac{1}{MN}\sum_{k=0}^{M-1}\sum_{l=0}^{N-1}\boldsymbol{\epsilon}^{kl}\exp\left(-2\pi\mathrm{i}\left(\frac{ku}{M}+\frac{lv}{N}\right)\right) = \frac{1}{MN}\sum_{k=0}^{M-1}\sum_{l=0}^{N-1}\boldsymbol{\epsilon}^{kl}\exp\left(-\mathrm{i}\theta_{uv}^{kl}\right), \tag{10}$$

with θ_{uv}^{kl} is the (k,l)-th angle in complex value space, and we may simplify it as θ^{kl} for ease of notations.

Next, we will show the proposition is a direct consequence of the concentration inequality of Gaussian distribution. We prove our results under one-dimensional Fourier transformation under dimension M, where the proof can be easily generalized to a two-dimensional case. Owing to the definition of the norm of complex value, for any specific u,

$$\|F_{\boldsymbol{\epsilon}}(u)\|^2 = F_{\boldsymbol{\epsilon}}(u)\overline{F_{\boldsymbol{\epsilon}}(u)} = \frac{1}{M^2}\boldsymbol{\epsilon}^\top\Lambda\mathbf{1}\mathbf{1}^\top\bar{\Lambda}\bar{\boldsymbol{\epsilon}}, \tag{11}$$

where $\Lambda = \mathrm{diag}(e^{-i\theta^0}, \cdots, e^{-i\theta^{M-1}})$. Then let $\boldsymbol{P} = (\sqrt{1/M}\mathbf{1}^\top, \cdots,)^\top\bar{\Lambda}$, where $(\sqrt{1/M}\mathbf{1}^\top, \cdots,)^\top$ is constructed by vector $\sqrt{1/M}\mathbf{1}$ and its orthogonal complement. We can verify that $\boldsymbol{P}$ is an orthogonal matrix. Then, let $\boldsymbol{\epsilon} = \boldsymbol{P}^\top\boldsymbol{y}$, so that $\boldsymbol{y}$ has the same distribution with $\boldsymbol{\epsilon}$. Thus

$$\frac{1}{M^2}\boldsymbol{\epsilon}^\top\Lambda\mathbf{1}\mathbf{1}^\top\bar{\Lambda}\boldsymbol{\epsilon} = \frac{1}{M^2}\boldsymbol{y}^\top\boldsymbol{P}\Lambda\mathbf{1}\mathbf{1}^\top\bar{\Lambda}\bar{\boldsymbol{P}}^\top\bar{\boldsymbol{y}} = \frac{1}{M}\boldsymbol{e}_1^\top\boldsymbol{y}\bar{\boldsymbol{y}}^\top\boldsymbol{e}_1 = \frac{1}{M}(\boldsymbol{y}^1)^2, \tag{12}$$

where $\boldsymbol{y}^1$ is a standard Gaussian. Thus, by the Berstein's inequality to sub-exponential random variable i.e., χ_1^2, we have

$$\mathbb{P}\left(|F_{\boldsymbol{\epsilon}}(u) - \mathbb{E}\left[F_{\boldsymbol{\epsilon}}(u)\right]| \geq \delta\right) = \mathbb{P}\left(\left|(\boldsymbol{y}^1)^2 - \mathbb{E}\left[(\boldsymbol{y}^1)^2\right]\right| \geq \delta\right) \leq 2\exp\left(-\frac{1}{8}\min\left\{\delta^2, \delta\right\}\right). \tag{13}$$

Since $\delta \in (0,1)$. Thus with probability at least $1 - \delta/M$, we have

$$\frac{1}{M} - \frac{1}{M}\sqrt{8\log\frac{2M}{\delta}} \leq \|F_{\boldsymbol{\epsilon}}(u)\|^2 \leq \frac{1}{M} + \frac{1}{M}\sqrt{8\log\frac{2M}{\delta}}, \tag{14}$$

which proves that the target $\|F_{\boldsymbol{\epsilon}_t}(u,v)\|^2$ is of order $\mathcal{O}(\frac{1}{M})$, so that verify our conclusion. $\square$

B Text-Image Alignment Metrics

In this paper, we mainly use three metrics as in [14] to measure the alignment between text prompt condition and generated image. Next, we give a brief introduction to the these metrics.

CLIPScore (Text). After extracting the features of generated images and text prompt respectively by CLIP encoder [30], CLIPScore (Text) is the cosine similarity between the two features. Similarly, the CLIPScore (Image) is the cosine-similarity between two image features.

BLIP-VQA. To improve the limited details capturing capability of the CLIP encoder, [14] propose BLIP-VQA which leverages the visual question answering (VQA) ability of BLIP model [18]. They compare the generated with the target text prompt separately described by several questions. For example, the prompt "A blue bird" can be separated into questions "a bird ?", "a blue bird ?" etc. Then BLIP-VQA outputs the probability of "Yes" when comparing generated images and these questions.

MiniGPT4-CoT. The MiniGPT4-CoT [14] combines a strong multi-modality question answering model MiniGPT-4 [51] and Chain-of-Thought [43]. The metric is computed by feeding the generated images to MiniGPT-4, then sequentially asking the model two questions "describe the image" and "predict the image-text alignment score". By constructing such CoT, the multi-modal model will not ignore the details in generated images.

14

C   Ablation Study on Number of [EOS]
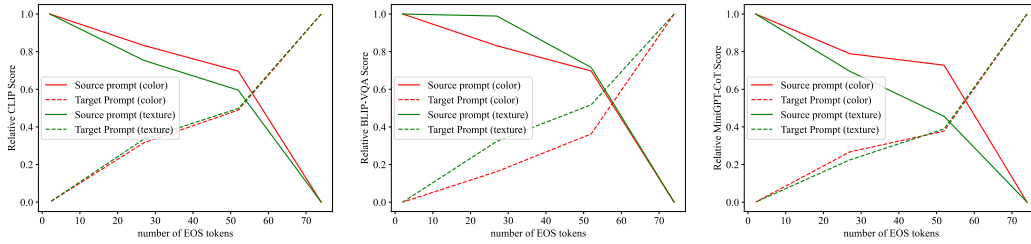
Figure 11: Relative BLIP-VQA Combine color and texture add complex, CLIP score, MiniGPT-CoT with source (or target) prompt under different number of [EOS]. Here the y-axis is the current BLIP-VQA, CLIP, MiniGPT-CoT over the maximum ones, which is used to alleviate the bias brought by the metric itself.

In this section, we conduct an ablation on the number of [EOS]. Concretely, for each text prompt in S-PromptSet, we repeat the semantic tokens in the text prompt e.g., "[SOS] + a yellow cat a yellow ... + [EOS]", so that the number of [EOS] is reduced in these constructed text prompts. Then, we generate images under these reconstructed text prompts and compare the text-image alignments between generated images and source or target prompts.

The results are in Figure 11. As can be seen, with the increasing of semantic tokens (so that decreasing of [EOS]), the generated images tend to be consistent with the source prompt, instead of the target prompt. Therefore, we speculate that the domination of [EOS] may be partially originated from its larger number, compared with semantic tokens. On the other hand, we observe that [EOS] in the forward positions have larger impacts compared to the latter ones, as the alignments between generated images with target prompts significantly decreased along the x-axis from right to left, in Figure 11. This trends further indicate that the [EOS] may contain more information compared with the latter ones, which indicates the domination of [EOS] originates from their larger number, but also the more information in the first few [EOS].

D   Conveyed Information in Semantic Tokens

During our discussion in Section 5, we conclude that the [EOS] has a larger impact than the ones of semantic tokens during T2I generation. However, as observed in Figure 4, under text prompt with switched [EOS], some information in semantic tokens are still conveyed in the generated images, e.g., blue color in the last image of the first row in Figure 4. Therefore, we explore how this information is conveyed in this section, which also reveals the working mechanism of text prompt.

Firstly, in Figure 12, we visualize the cross-attention map of each tokens under text prompt from S-PromptSet, similar to Figure 1b. Surprisingly, we find that in cross-attention map of semantic tokens and [EOS] are all visually similar to the shape of the final generated images. The similarity is reasonable for [EOS] as it contains the overall information, so that it is perceptible and transfer their information according to constructed cross-attention map.

On the other hand, when semantic tokens convey their information according to the similar cross-attention, for attributes (color or texture), unlike object information, they are potentially not contradict to overall shape decided by [EOS]. Thus, the information of attributes is more likely to be conveyed in its corresponding pixels. However, this does hold for object/noun tokens whose information is very likely related to shape, which has already been decided by [EOS].

This discussion explains the phenomenon of information in semantic tokens are appeared in the generated images under prompt from S-PromptSet. Combining the observations to the working stage of text prompt in Section 5, we can conclude that the semantic tokens also work in the T2I generation, though it has less impact compared to [EOS].

15
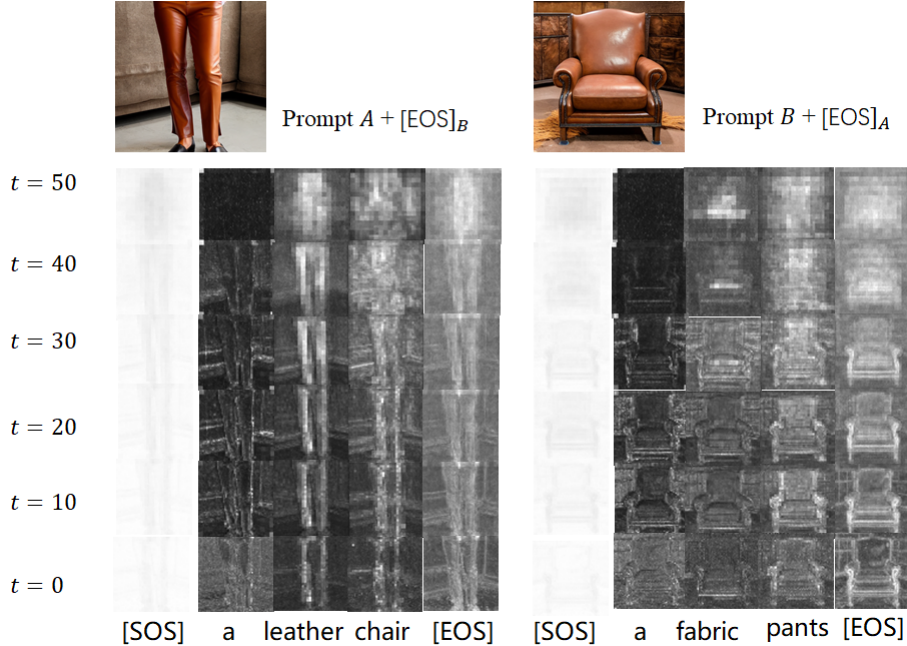
Figure 12: The visualization of cross-attention map under text prompt with switched [EOS] from S-PromptSet. The pixels corresponding to semantic tokens are in the shape of the final generated data as in text prompt B provide [EOS]. For example, the token "chair" corresponds to pixels in the shape of paint, so its information can not be conveyed, while this phenomenon does exist in the attribute token "leather".

Figure 13: Generated images with prompts only contain information from [SOS] or [EOS].

E [SOS] Contains no Textual Information

As mentioned in Section 5.1, the special token [SOS] is supposed to contain no textual information, due to the auto-regressive textual prompt encoder. To further verify this, we conduct the following two types of prompts. 1): all 77 tokens are [SOS] from the given text prompt, 2) except the first [SOS] token, all other 76 tokens are [EOS] from the given text prompt. Then, we generate images under these prompts with SD v1.5. The generated images as in Figure 13. As can be seen, for the first type of prompt, no textual information is conveyed, while the phenomenon disappears in the second type of prompt. This observation verifies our conclusion that [SOS] contains no textual information.

16

Sem+EOS	Sem+Zero	Zero+EOS	Sem+Rand	Rand+EOS
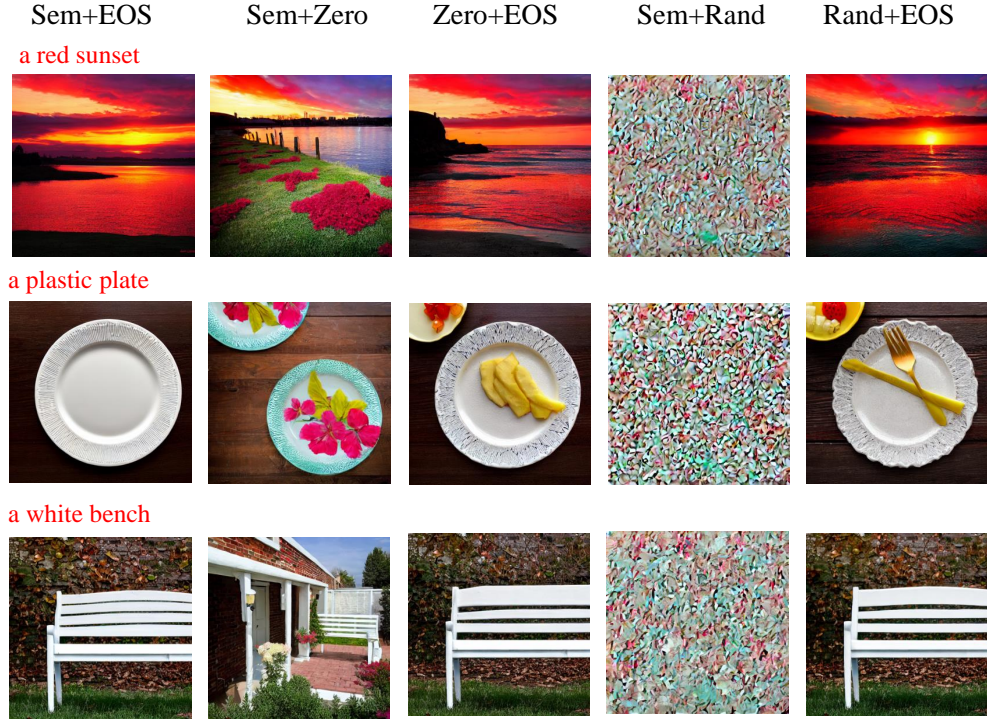
Figure 14: Generated images with zero or random vectors substitution.

Table 3: The alignment of generated results image under different constructed text prompt sets. Here "Sem + EOS" is the original text prompt, and serves as baseline here. Besides that, the CLIPScore (Image) is the image-level alignment of generated images with the ones under "Sem + EOS".

Text Prompt	CLIPScore (Text)↑	CLIPScore (Image)↑	BLIP-VQA↑	MiniGPT4-CoT↑
Sem + Zero	0.2407	0.6732	0.5392	0.6757
Sem + Rand	0.2153	0.6038	0.3606	0.5428
Zero + EOS	0.2999	0.8887	0.7467	0.6982
Rand + EOS	0.3008	0.8791	0.7669	0.7000
Sem + EOS	0.3110	1.0000	0.8999	0.7412

F More Evidences on [EOS] Contains More Information

In this section, we further verify that the impact of [EOS] is larger than the ones of semantic tokens in T2I generation. To further verify this conclusion, under the text prompts with the format of "[SOS] + Sem + [EOS]" from our dataset PromptSet, we substitute all semantic tokens or [EOS] with zero vectors or random Gaussian noise. As a result, we get the 4 sets of text prompts, i.e., "[SOS] + Sem + Zero" (abbrev Sem + Zero), "[SOS] + Sem + Random" (Sem + Rand), "[SOS] + Zero + [EOS]" (Zero + EOS), and "[SOS] + Random + [EOS]" (Rand + EOS). These constructed text prompts ideally contain complete semantic information, and we verify the alignment of the generated images with the corresponding text prompt conditions. The alignments are measured by text-image alignment metrics: CLIPScore [30, 10], BLIP-VQA [18, 14], and MiniGPT4-CoT [51, 14].

The results are summarized in Table 3. As can be seen, as expected for baseline combination "Sem + EOS", the alignments under text prompts with "EOS" preserved are significantly better than the ones with "Sem" preserved. Thus, the observations further verify our conclusion that *the [EOS] has larger influences than semantic tokens during the denoising process.*

Moreover, we find the generation is somehow robust, as involving random noise in text prompts still generates semantic meaningful images. We visualize some generated images under constructed text-

17

Table 4: The alignment of generated image with its source and target prompts, under switched `[EOS]` on Key or Value substitution. Here KV-Sub is the complete substitution as in Section 5, which serves as a baseline here.

Attribute Alignment	K-Sub Source	K-Sub Target	V-Sub Source	V-Sub Target	KV-Sub Source	KV-Sub Target
CLIPScore (Text)↑	**0.3132**	0.1875	0.2538	**0.2628**	0.2363	**0.2758**
BLIP-VQA↑	**0.7127**	0.2379	0.3724	**0.3984**	0.3325	**0.4441**
MiniGPT-CoT↑	**0.8025**	0.6215	0.6749	**0.7071**	0.6473	**0.7213**

prompts from Table 3 in Figure 14, which indicates the images under "Zero + EOS" indeed visually have the best quality in alignment, so that consist with Table 3. Besides that, the other combinations generate semantic meaningful images as well, expected for "Sem + Rand" Thus semantic tokens do not contain enough information for generation.

G Key or Value Dominates the Influence?
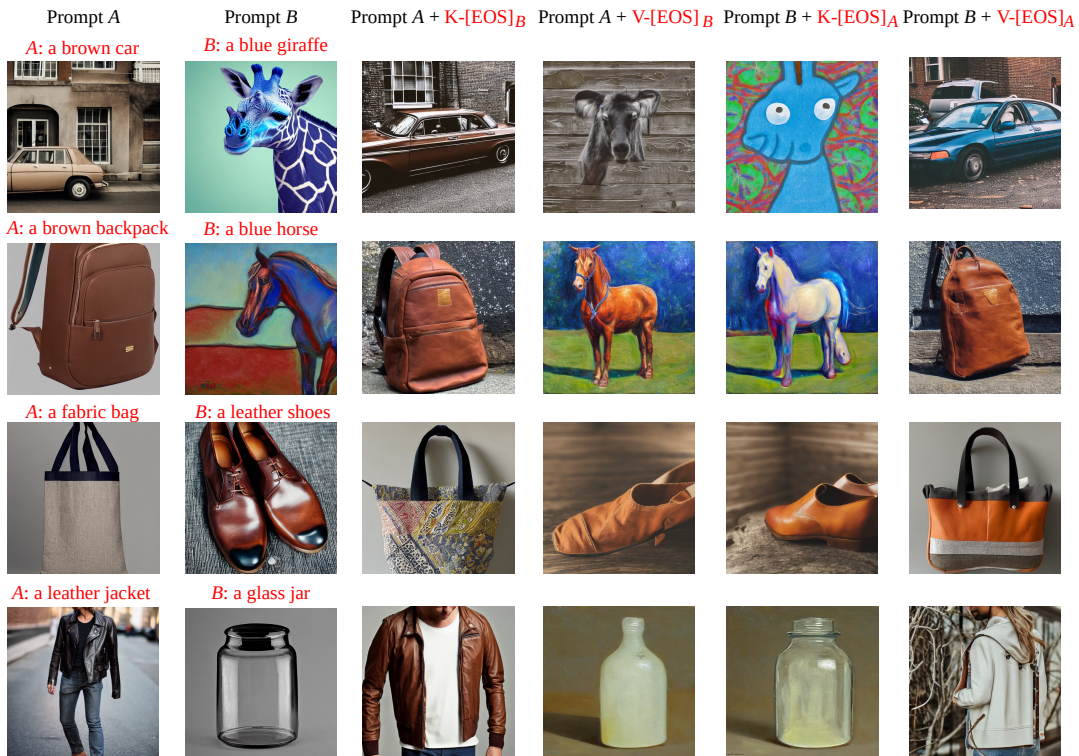
Figure 15: Generated examples of Key or Value substitution.

As mentioned in Section 3, the information from `[EOS]` is conveyed by the cross-attention module. More concretely, the Key (K) and Value (V) in it, respectively decide the weights and features in the output of the cross-attention module (a weighted sum of features). Next, we explore their individual influence for `[EOS]` to further reveal the working mechanism of it.

Concretely, as in Section 5, we generate images under the constructed text prompt set `S-PromptSet`. However, the substitution of `[EOS]` is only conducted on computing Key or Values in cross-attention module, which are respectively denoted as K-Substitution (Sub) and V-Sub. For such two substitutions, similar to Table 1, we compare the image-text alignment of generated images with source and target prompts.

18
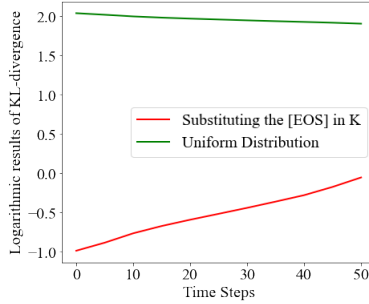
Figure 16: The averaged KL-divergence over pixels and layers.
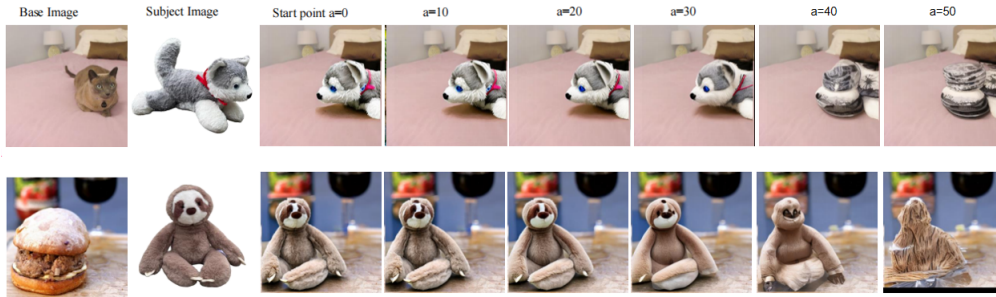
Figure 17: We implement our sampling strategy on subject-driven generation model, AnyDoor [44]. We remove the condition image from different time steps (denote as a) during denoising process. The generated images still preserve the specific details as baseline model (start point $a = 0$) when start removing time steps is set to 20.
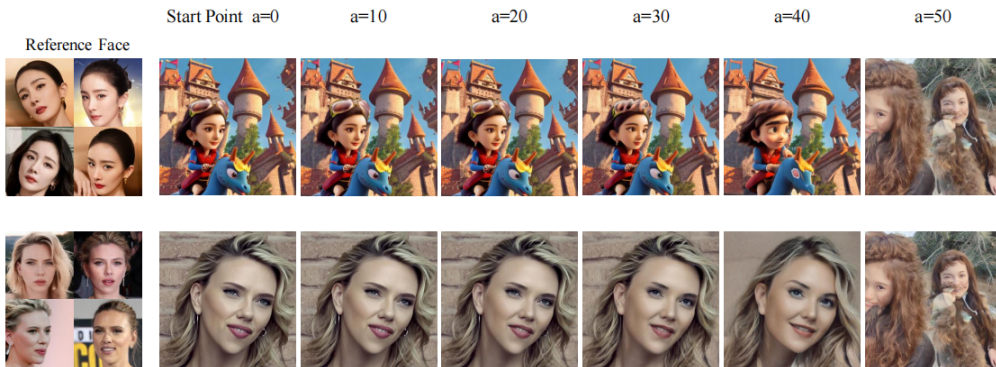
Figure 18: We implement our sampling strategy on human face generation model, PhotoMaker. We remove the condition (text prompts and reference face) from different time steps (denote as a) during denoising process. The generated images and faces still preserve the specific details as baseline model (start point $a = 0$) when start removing time steps is set to 20.

The results are summarized in Table 4. As can be seen, substituting the [EOS] in V has a larger influence than the substitutions in K. To explain this, as we have observed in Figure 3, the weights on semantic tokens and [EOS] are significantly smaller than the ones on [SOS]. However, the K of [EOS] is only related to these small weights, which have limited influence. In contrast to K, the V of [EOS] contains information on features, which can be directly conveyed in generated images. So that we can conclude the value of [EOS] dominates the influence in generation as observed in Table 4. We present some generated images under text prompts from S-PromptSet, but with only Key or Value substituted as in Table 4. The generated images are in Figure 15.

19

Prompt A: The warm, golden glow of the sunrise lit up the horizon, a natural wonder of breathtaking beauty.
Prompt B: The sharp, pointed teeth of the shark contrasted with its sleek, streamlined body, a powerful and graceful predator of the ocean.

Prompt A: A brown cow.
Prompt B: A red suitcase.

Prompt A: A fabric towel.
Prompt B: A glass vase.

Prompt A: A fabric pants.
Prompt B: A leather wallet.

Figure 19: More generated examples under tokens from `S-PromptSet`.

We further verify the variation of the cross-attention map after substituting [EOS]. For each pixel, the cross-attention map of it is a discrete probability distribution. Thus, we compute the KL-divergence [41] between probability distributions under substituted/unsubstituted K. The averaged KL-divergence over pixels and layers in models under different denoising steps is presented in Figure 16, where we add the KL-divergence of cross-attention map distribution between a uniform distribution as a baseline. The result shows that even with substituted [EOS], the cross-attention map does not vary much. We speculate that this is because as in Figure 3, the weights in [SOS] dominate the cross-attention map. Thus, in the cross-attention module, altering K has a slighter influence compared with altering V.

H Firstly Conveyed Information for Subject-Driven Generation

As mentioned in Section 5.1, the injected textual information is conveyed in the first stage of diffusion model. Since the information is conveyed in the cross-attention module of model, we speculate this phenomenon may be generalized to the other conditional generation task, e.g., subject-driven generation with an extra image as condition.

20

To see this, we conduct experiments under two tasks: zero-shot subject-driven generation and human face generation. For such two tasks, there is extra reference image (given subject and human face) used as condition to guide image generation. We use the sampling strategy as in Figure 10 for the two tasks, respectively follow the backbone methods AnyDoor [44] and Photomaker [50]. The results are in Figures 17 and 18, respectively.

As can be seen, the generation results verify the conclusion that for conditional information from in the other modality than text, they will be also firstly conveyed in during the diffusion process.

I   More Generated Images

I.1   [EOS] Substitution

In this subsection, we first present the generated images under text prompts from S-PromptSet in Figure 19. As can be seen, most overall shape of generated images are consistent with the ones conveyed by [EOS].

I.2   Generated Images in Paragraph "Acceleration of Sampling" of Section 6

Next, we present more generated images under noise prediction (9) with varied a in Figure 20 and 21.
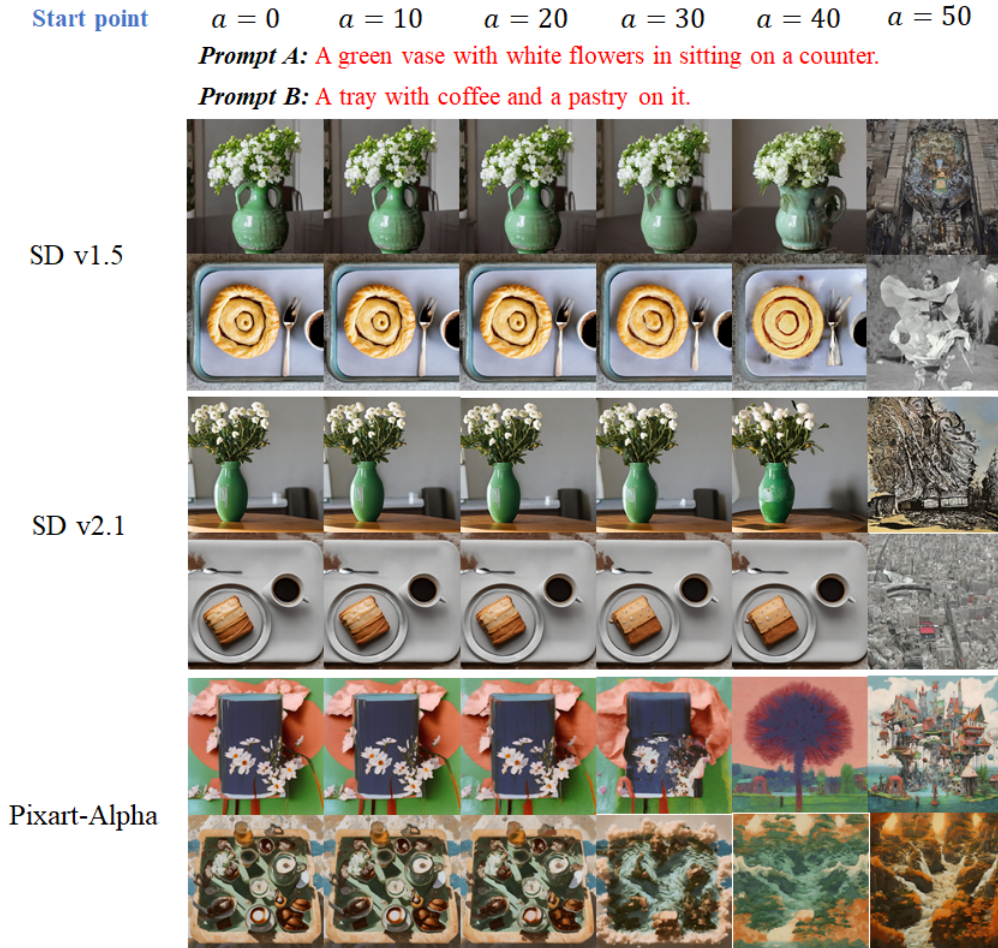
Figure 20: The generated images with 50 steps DDIM under ϵ_θ in (9), where the textual information are $\mathcal{C}$ removed during time steps $t \in [0, a]$. With $a \to 50$, the inference cost is decreased.

21

Start point $a = 0$ $a = 5$ $a = 10$ $a = 15$ $a = 20$ $a = 25$

Prompt A: A kitchen counter is lined with multiple objects..

Prompt B: A plate with some vegetables and meat on it.

SD v1.5

SD v2.1

Pixart-Alpha
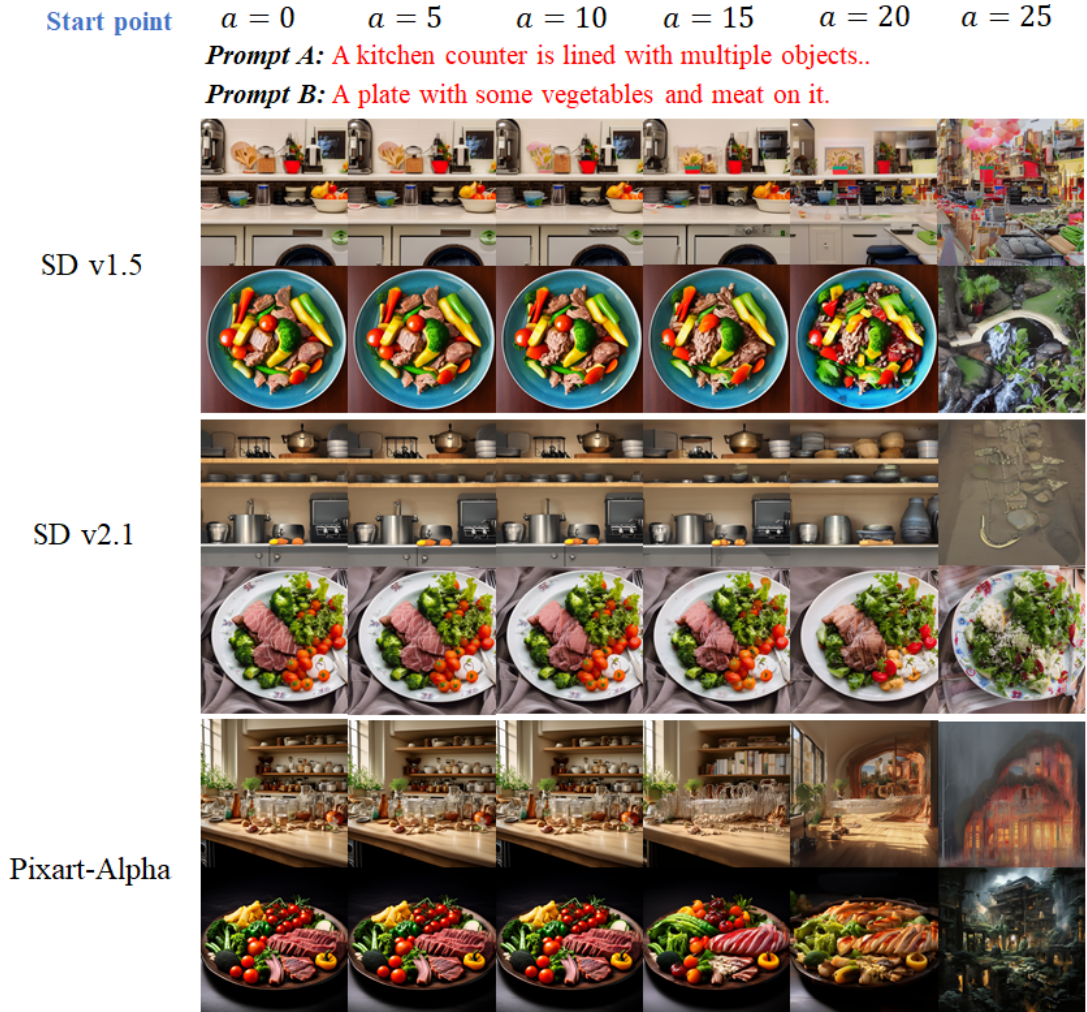
Figure 21: More generated images with 25 steps DPM-Solver under ϵ_θ in (9), where the textual information are $\mathcal{C}$ removed during time steps $t \in [0, a]$. With $a \to 25$, the inference cost is decreased.

NeurIPS Paper Checklist

1. **Claims**

   Question: Do the main claims made in the abstract and introduction accurately reflect the paper's contributions and scope?

   Answer: [Yes]

   Justification: The main contributions of this paper have been clarified in Abstract.

   Guidelines:

   - The answer NA means that the abstract and introduction do not include the claims made in the paper.
   - The abstract and/or introduction should clearly state the claims made, including the contributions made in the paper and important assumptions and limitations. A No or NA answer to this question will not be perceived well by the reviewers.
   - The claims made should match theoretical and experimental results, and reflect how much the results can be expected to generalize to other settings.
   - It is fine to include aspirational goals as motivation as long as it is clear that these goals are not attained by the paper.

22

2. **Limitations**

   Question: Does the paper discuss the limitations of the work performed by the authors?

   Answer: [Yes]

   Justification: The limitation of this paper is discussed in the main paper.

   Guidelines:

   - The answer NA means that the paper has no limitation while the answer No means that the paper has limitations, but those are not discussed in the paper.
   - The authors are encouraged to create a separate "Limitations" section in their paper.
   - The paper should point out any strong assumptions and how robust the results are to violations of these assumptions (e.g., independence assumptions, noiseless settings, model well-specification, asymptotic approximations only holding locally). The authors should reflect on how these assumptions might be violated in practice and what the implications would be.
   - The authors should reflect on the scope of the claims made, e.g., if the approach was only tested on a few datasets or with a few runs. In general, empirical results often depend on implicit assumptions, which should be articulated.
   - The authors should reflect on the factors that influence the performance of the approach. For example, a facial recognition algorithm may perform poorly when image resolution is low or images are taken in low lighting. Or a speech-to-text system might not be used reliably to provide closed captions for online lectures because it fails to handle technical jargon.
   - The authors should discuss the computational efficiency of the proposed algorithms and how they scale with dataset size.
   - If applicable, the authors should discuss possible limitations of their approach to address problems of privacy and fairness.
   - While the authors might fear that complete honesty about limitations might be used by reviewers as grounds for rejection, a worse outcome might be that reviewers discover limitations that aren't acknowledged in the paper. The authors should use their best judgment and recognize that individual actions in favor of transparency play an important role in developing norms that preserve the integrity of the community. Reviewers will be specifically instructed to not penalize honesty concerning limitations.

3. **Theory Assumptions and Proofs**

   Question: For each theoretical result, does the paper provide the full set of assumptions and a complete (and correct) proof?

   Answer: [NA]

   Justification:

   Guidelines:

   - The answer NA means that the paper does not include theoretical results.
   - All the theorems, formulas, and proofs in the paper should be numbered and cross-referenced.
   - All assumptions should be clearly stated or referenced in the statement of any theorems.
   - The proofs can either appear in the main paper or the supplemental material, but if they appear in the supplemental material, the authors are encouraged to provide a short proof sketch to provide intuition.
   - Inversely, any informal proof provided in the core of the paper should be complemented by formal proofs provided in appendix or supplemental material.
   - Theorems and Lemmas that the proof relies upon should be properly referenced.

4. **Experimental Result Reproducibility**

   Question: Does the paper fully disclose all the information needed to reproduce the main experimental results of the paper to the extent that it affects the main claims and/or conclusions of the paper (regardless of whether the code and data are provided or not)?

   Answer: [Yes]

23

Justification: The experimental details are in main part of this paper.

Guidelines:

- The answer NA means that the paper does not include experiments.
- If the paper includes experiments, a No answer to this question will not be perceived well by the reviewers: Making the paper reproducible is important, regardless of whether the code and data are provided or not.
- If the contribution is a dataset and/or model, the authors should describe the steps taken to make their results reproducible or verifiable.
- Depending on the contribution, reproducibility can be accomplished in various ways. For example, if the contribution is a novel architecture, describing the architecture fully might suffice, or if the contribution is a specific model and empirical evaluation, it may be necessary to either make it possible for others to replicate the model with the same dataset, or provide access to the model. In general. releasing code and data is often one good way to accomplish this, but reproducibility can also be provided via detailed instructions for how to replicate the results, access to a hosted model (e.g., in the case of a large language model), releasing of a model checkpoint, or other means that are appropriate to the research performed.
- While NeurIPS does not require releasing code, the conference does require all submissions to provide some reasonable avenue for reproducibility, which may depend on the nature of the contribution. For example
  (a) If the contribution is primarily a new algorithm, the paper should make it clear how to reproduce that algorithm.
  (b) If the contribution is primarily a new model architecture, the paper should describe the architecture clearly and fully.
  (c) If the contribution is a new model (e.g., a large language model), then there should either be a way to access this model for reproducing the results or a way to reproduce the model (e.g., with an open-source dataset or instructions for how to construct the dataset).
  (d) We recognize that reproducibility may be tricky in some cases, in which case authors are welcome to describe the particular way they provide for reproducibility. In the case of closed-source models, it may be that access to the model is limited in some way (e.g., to registered users), but it should be possible for other researchers to have some path to reproducing or verifying the results.

5. **Open access to data and code**

   Question: Does the paper provide open access to the data and code, with sufficient instructions to faithfully reproduce the main experimental results, as described in supplemental material?

   Answer: [No]

   Justification: We will release the code in future.

   Guidelines:

   - The answer NA means that paper does not include experiments requiring code.
   - Please see the NeurIPS code and data submission guidelines (`https://nips.cc/public/guides/CodeSubmissionPolicy`) for more details.
   - While we encourage the release of code and data, we understand that this might not be possible, so "No" is an acceptable answer. Papers cannot be rejected simply for not including code, unless this is central to the contribution (e.g., for a new open-source benchmark).
   - The instructions should contain the exact command and environment needed to run to reproduce the results. See the NeurIPS code and data submission guidelines (`https://nips.cc/public/guides/CodeSubmissionPolicy`) for more details.
   - The authors should provide instructions on data access and preparation, including how to access the raw data, preprocessed data, intermediate data, and generated data, etc.
   - The authors should provide scripts to reproduce all experimental results for the new proposed method and baselines. If only a subset of experiments are reproducible, they should state which ones are omitted from the script and why.

24

- At submission time, to preserve anonymity, the authors should release anonymized versions (if applicable).
- Providing as much information as possible in supplemental material (appended to the paper) is recommended, but including URLs to data and code is permitted.

6. **Experimental Setting/Details**

Question: Does the paper specify all the training and test details (e.g., data splits, hyper-parameters, how they were chosen, type of optimizer, etc.) necessary to understand the results?

Answer: [Yes]

Justification: They are specified in main part of this paper.

Guidelines:

- The answer NA means that the paper does not include experiments.
- The experimental setting should be presented in the core of the paper to a level of detail that is necessary to appreciate the results and make sense of them.
- The full details can be provided either with the code, in appendix, or as supplemental material.

7. **Experiment Statistical Significance**

Question: Does the paper report error bars suitably and correctly defined or other appropriate information about the statistical significance of the experiments?

Answer: [NA]

Justification: The results have no error bars.

Guidelines:

- The answer NA means that the paper does not include experiments.
- The authors should answer "Yes" if the results are accompanied by error bars, confidence intervals, or statistical significance tests, at least for the experiments that support the main claims of the paper.
- The factors of variability that the error bars are capturing should be clearly stated (for example, train/test split, initialization, random drawing of some parameter, or overall run with given experimental conditions).
- The method for calculating the error bars should be explained (closed form formula, call to a library function, bootstrap, etc.)
- The assumptions made should be given (e.g., Normally distributed errors).
- It should be clear whether the error bar is the standard deviation or the standard error of the mean.
- It is OK to report 1-sigma error bars, but one should state it. The authors should preferably report a 2-sigma error bar than state that they have a 96% CI, if the hypothesis of Normality of errors is not verified.
- For asymmetric distributions, the authors should be careful not to show in tables or figures symmetric error bars that would yield results that are out of range (e.g. negative error rates).
- If error bars are reported in tables or plots, The authors should explain in the text how they were calculated and reference the corresponding figures or tables in the text.

8. **Experiments Compute Resources**

Question: For each experiment, does the paper provide sufficient information on the computer resources (type of compute workers, memory, time of execution) needed to reproduce the experiments?

Answer: [Yes]

Justification:

Guidelines:

- The answer NA means that the paper does not include experiments.

25

- The paper should indicate the type of compute workers CPU or GPU, internal cluster, or cloud provider, including relevant memory and storage.
- The paper should provide the amount of compute required for each of the individual experimental runs as well as estimate the total compute.
- The paper should disclose whether the full research project required more compute than the experiments reported in the paper (e.g., preliminary or failed experiments that didn't make it into the paper).

9. **Code Of Ethics**

Question: Does the research conducted in the paper conform, in every respect, with the NeurIPS Code of Ethics `https://neurips.cc/public/EthicsGuidelines`?

Answer: [Yes]

Justification:

Guidelines:

- The answer NA means that the authors have not reviewed the NeurIPS Code of Ethics.
- If the authors answer No, they should explain the special circumstances that require a deviation from the Code of Ethics.
- The authors should make sure to preserve anonymity (e.g., if there is a special consideration due to laws or regulations in their jurisdiction).

10. **Broader Impacts**

Question: Does the paper discuss both potential positive societal impacts and negative societal impacts of the work performed?

Answer: [NA]

Justification:

Guidelines:

- The answer NA means that there is no societal impact of the work performed.
- If the authors answer NA or No, they should explain why their work has no societal impact or why the paper does not address societal impact.
- Examples of negative societal impacts include potential malicious or unintended uses (e.g., disinformation, generating fake profiles, surveillance), fairness considerations (e.g., deployment of technologies that could make decisions that unfairly impact specific groups), privacy considerations, and security considerations.
- The conference expects that many papers will be foundational research and not tied to particular applications, let alone deployments. However, if there is a direct path to any negative applications, the authors should point it out. For example, it is legitimate to point out that an improvement in the quality of generative models could be used to generate deepfakes for disinformation. On the other hand, it is not needed to point out that a generic algorithm for optimizing neural networks could enable people to train models that generate Deepfakes faster.
- The authors should consider possible harms that could arise when the technology is being used as intended and functioning correctly, harms that could arise when the technology is being used as intended but gives incorrect results, and harms following from (intentional or unintentional) misuse of the technology.
- If there are negative societal impacts, the authors could also discuss possible mitigation strategies (e.g., gated release of models, providing defenses in addition to attacks, mechanisms for monitoring misuse, mechanisms to monitor how a system learns from feedback over time, improving the efficiency and accessibility of ML).

11. **Safeguards**

Question: Does the paper describe safeguards that have been put in place for responsible release of data or models that have a high risk for misuse (e.g., pretrained language models, image generators, or scraped datasets)?

Answer: [NA]

Justification:

26

Guidelines:

- The answer NA means that the paper poses no such risks.
- Released models that have a high risk for misuse or dual-use should be released with necessary safeguards to allow for controlled use of the model, for example by requiring that users adhere to usage guidelines or restrictions to access the model or implementing safety filters.
- Datasets that have been scraped from the Internet could pose safety risks. The authors should describe how they avoided releasing unsafe images.
- We recognize that providing effective safeguards is challenging, and many papers do not require this, but we encourage authors to take this into account and make a best faith effort.

12. **Licenses for existing assets**

    Question: Are the creators or original owners of assets (e.g., code, data, models), used in the paper, properly credited and are the license and terms of use explicitly mentioned and properly respected?

    Answer: [NA]

    Justification:

    Guidelines:

    - The answer NA means that the paper does not use existing assets.
    - The authors should cite the original paper that produced the code package or dataset.
    - The authors should state which version of the asset is used and, if possible, include a URL.
    - The name of the license (e.g., CC-BY 4.0) should be included for each asset.
    - For scraped data from a particular source (e.g., website), the copyright and terms of service of that source should be provided.
    - If assets are released, the license, copyright information, and terms of use in the package should be provided. For popular datasets, `paperswithcode.com/datasets` has curated licenses for some datasets. Their licensing guide can help determine the license of a dataset.
    - For existing datasets that are re-packaged, both the original license and the license of the derived asset (if it has changed) should be provided.
    - If this information is not available online, the authors are encouraged to reach out to the asset's creators.

13. **New Assets**

    Question: Are new assets introduced in the paper well documented and is the documentation provided alongside the assets?

    Answer: [NA]

    Justification:

    Guidelines:

    - The answer NA means that the paper does not release new assets.
    - Researchers should communicate the details of the dataset/code/model as part of their submissions via structured templates. This includes details about training, license, limitations, etc.
    - The paper should discuss whether and how consent was obtained from people whose asset is used.
    - At submission time, remember to anonymize your assets (if applicable). You can either create an anonymized URL or include an anonymized zip file.

14. **Crowdsourcing and Research with Human Subjects**

    Question: For crowdsourcing experiments and research with human subjects, does the paper include the full text of instructions given to participants and screenshots, if applicable, as well as details about compensation (if any)?

27

Answer: [NA]

Justification:

Guidelines:

- The answer NA means that the paper does not involve crowdsourcing nor research with human subjects.
- Including this information in the supplemental material is fine, but if the main contribution of the paper involves human subjects, then as much detail as possible should be included in the main paper.
- According to the NeurIPS Code of Ethics, workers involved in data collection, curation, or other labor should be paid at least the minimum wage in the country of the data collector.

15. **Institutional Review Board (IRB) Approvals or Equivalent for Research with Human Subjects**

Question: Does the paper describe potential risks incurred by study participants, whether such risks were disclosed to the subjects, and whether Institutional Review Board (IRB) approvals (or an equivalent approval/review based on the requirements of your country or institution) were obtained?

Answer: [NA]

Justification:

Guidelines:

- The answer NA means that the paper does not involve crowdsourcing nor research with human subjects.
- Depending on the country in which research is conducted, IRB approval (or equivalent) may be required for any human subjects research. If you obtained IRB approval, you should clearly state this in the paper.
- We recognize that the procedures for this may vary significantly between institutions and locations, and we expect authors to adhere to the NeurIPS Code of Ethics and the guidelines for their institution.
- For initial submissions, do not include any information that would break anonymity (if applicable), such as the institution conducting the review.

28